Table 9.1.7.3. *Space groups with alternative, non-equivalent indexing schemes*

Symmetry operations required for re-indexing are given as relations of indices and in the matrix form. In brackets are the chiral pairs of space groups indistinguishable by diffraction. These space groups may also display the effect of merohedral twinning, with the twinning symmetry operators the same as those required for re-indexing.

Space group	Re-indexing transformation	
$P4$, $(P4_1, P4_3)$, $P4_2$, $I4$, $I4_1$	$hkl \rightarrow kh\bar{l}$	$010/100/00\bar{1}$
$P3$, $(P3_1, P3_2)$	$hkl \rightarrow \bar{h}\bar{k}l$	$\bar{1}00/0\bar{1}0/001$
	or $hkl \rightarrow kh\bar{l}$	$010/100/00\bar{1}$
	or $hkl \rightarrow \bar{k}\bar{h}\bar{l}$	$0\bar{1}0/\bar{1}00/00\bar{1}$
$R3$	$hkl \rightarrow kh\bar{l}$	$010/100/00\bar{1}$
$P321$, $(P3_121, P3_221)$	$hkl \rightarrow \bar{h}\bar{k}l$	$\bar{1}00/0\bar{1}0/001$
$P312$, $(P3_112, P3_212)$	$hkl \rightarrow \bar{h}\bar{k}l$	$\bar{1}00/0\bar{1}0/001$
$P6$, $(P6_1, P6_5)$, $(P6_2, P6_4)$, $P6_3$	$hkl \rightarrow kh\bar{l}$	$010/100/00\bar{1}$
$P23$, $P2_13$, $(I23, I2_13)$, $F23$	$hkl \rightarrow k\bar{h}l$	$010/\bar{1}00/001$

However, under alternative indexing schemes, the same reflection will be given different indices, which can pose problems when data from more than one crystal are to be merged or compared. Merging is needed when more than one sample is required to record a complete data set. Comparison is needed when looking for heavy-atom derivatives or for ligand complexes with isomorphous crystals. For these, the reflections of one crystal must be selected as a standard, and it is easy to make other crystals consistent with this standard either by changing the orientation matrix at the time of intensity integration or by applying re-indexing to the integrated intensity set. The alternative indexing schemes are related by those symmetry operations present within the higher symmetry of the Bravais lattice but absent from the point-group symmetry. The point groups with alternative indexing systems are shown in Table 9.1.7.3, together with the necessary symmetry operations for re-indexing.

Several experiments require the recording of multiple data sets from the same crystal. One example is the collection of more than one pass with different exposure times (see below), and a second is in multiwavelength anomalous dispersion (MAD) experiments. In these experiments, the software systems may independently choose any of the alternative systems for different sets, which may then be incompatible and need re-indexing. It is much simpler to ensure a common orientation matrix modified as appropriate for all sets at the time of intensity integration.

9.1.8. Crystal-to-detector distance

The crystal-to-detector distance (CTDD) should be selected so that the whole area of the detector is usefully exploited. The shorter the CTDD, the higher the resolution of the indexed reflections at the edge of the image; but if the CTDD is too short, then the outer regions of the detector window record only indices with attached noise rather than intensities. A longer CTDD spreads the background radiation over a larger area of the detector as the background level diminishes in proportion to the square of the CTDD. In contrast, owing to collimation and focusing, the profiles of the Bragg reflections do not broaden so much, and the signal-to-noise ratio is enhanced at longer distances. It is advantageous to use the largest possible CTDD while ensuring that meaningful data are not lost beyond the active edge of the detector.

It is not straightforward to judge the resolution limit of meaningful diffraction. The most scientific approach involves recording, processing and merging a small number of images and making a decision on the basis of the resulting intensity statistics. However, this does require time, which should only pose a problem on ultra high intensity sources with very rapid data collection. A more pragmatic approach relies on visual inspection of the initial exposures using a graphical display at various contrast levels. Normally, if reflections are not visible by eye at the highest display contrast, their intensities are not meaningful. Some safety margin can be applied by setting the CTDD to a slightly shorter value than that estimated from visual inspection. Naturally, the resolution limit to which meaningful intensities extend depends on the exposure time, and the decision concerning the CTDD should follow the selection of the appropriate exposure (Section 9.1.11.2).

In addition to the significance of the reflection intensities, another important factor is the spatial resolution of spot profiles on the detector. If the crystal cell dimensions are large, the profiles may superimpose and the reflections may be impossible to integrate. At longer CTDD, the diffraction pattern spreads out and the profile overlap diminishes. If necessary, the detector can be offset from the central position to measure high-resolution data at long CTDD, but a larger total rotation is required to reach full data completeness. This applies only if the overlap of profiles belonging to the same lune results from a long axis lying parallel to the detector plane. The superposition of reflection profiles resulting from overlapping lunes will not be alleviated by increasing the CTDD; the only remedy for this is to reduce the rotation range $\Delta\varphi$ per exposure.

In addition to the proper selection of the CTDD, attention should be given to the proper positioning of the beam stop. It should be centred with respect to the direct beam and cover the beam cross section completely. No part of the direct beam should reach the detector, and there should be no indirect scatter by the beam stop. The optimal reduction of air scatter is to have the smallest beam stop consistent with the dimensions of the beam, placed as close as possible to the crystal. For a given size of beam stop, the crystal-to-beam stop distance should be matched to the CTDD, sufficiently far from the crystal to minimize its shadow and concomitant obstruction of the valuable lowest-resolution reflections. If the beam stop is mounted on a metal wire, it is better to position the wire along the spindle axis where it will only interfere with those reflections around the blind region.

9.1.9. Wavelength

The wavelength of X-radiation can be tuned only at synchrotron sources. Rotating-anode generators produce radiation at a fixed wavelength which is characteristic of the metal of the anode, usually copper with $\lambda = 1.542$ Å.

The proper selection of the wavelength is most important for collecting data containing an anomalous-scattering signal. In general, the imaginary component $\Delta f''$ of the anomalous-dispersion signal is high on the short-wavelength side of the absorption edge of the anomalous scatterer present in the crystal. Near the absorption edge, both components, real $\Delta f'$ and imaginary $\Delta f''$, vary significantly. This variation is utilized in the MAD technique, the strict requirements of which are discussed in Chapter 14.2.

If the data are collected using a single wavelength with the aim of measuring Bijvoet differences, $\Delta F_{\rm anom} = F^+ - F^-$, the requirements are not as strict as for MAD. However, it may be advisable to record the fluorescence spectrum around the region of the expected absorption edge. If the fluorescence signal from the crystalline sample is too weak, the appropriate metal or salt standard can be used. However, the chemical environment of the anomalous scatterers may cause a shift of the edge by up to 10 eV, and it is

safer to use a wavelength which is 0.001–0.002 Å shorter (or use an energy 10–20 eV higher) than the edge recorded from the standard. When using anomalous scatterers displaying large white lines within their spectra, the wavelength should be accurately adjusted on the basis of the spectrum measured from the actual sample.

For collecting data without an anomalous signal, there are no strict requirements concerning the wavelength. The maximum intensity provided by the beamline depends on the energy of particles in the synchrotron storage ring and on the beamline optics. Typically, wavelengths around 1 Å or shorter are used at most synchrotrons, assuring high beam intensity and low absorption of X-rays by the sample and air, thus reducing the radiation damage of the crystal. This is of particular importance at the very bright beamlines at third-generation synchrotrons. To diminish the effect of air absorption further, it is possible to fill the space between the crystal and the detector with helium. Short wavelengths are advantageous for collecting high-resolution data, since the diffraction angles are smaller and there is no need to use a very short CTDD. The effect of profile elongation owing to the oblique incidence of diffracted X-ray beams on the detector is then smaller, and the blind region is narrower.

9.1.10. Lysozyme as an example

Tetragonal hen egg-white lysozyme (Chapter 26.1 and Blake *et al.*, 1967), crystallizing in the space group $P4_32_12$ with cell dimensions $a = b = 78.6$ and $c = 37.2$ Å, is used here as a model system to illustrate some of the points made above, based on Dauter (1999). The example involves a set of two consecutive blocks of images with a crystal-to-detector distance of 243 mm, a wavelength of 0.92 Å, a resolution of 2.7 Å, an oscillation range of 1.5° and a crystal mosaicity around 0.5°. These images are shown in Fig. 9.1.10.1(*a–f*).

The first four images, (*a–d*), were exposed with the tetragonal fourfold *c* axis lying approximately along the direction of the beam. On these images, the reflections within each lune are arranged in a square grid, reflecting the tetragonal symmetry with $a = b$. The squares are oriented with their diagonals in the horizontal and vertical directions of the image, as the crystal was mounted with its [110] direction along the spindle rotation axis. Indeed, at the end of image (*a*) and the start of image (*b*), the *c* axis lay almost perfectly along the beam, and the zero-layer lune almost disappears behind the beam-stop shadow, since the corresponding (*hk*0) plane in reciprocal space is tangential to the Ewald sphere at the origin of the reciprocal lattice.

The lunes are widely spaced with clear gaps between them, because the third cell dimension, *c*, which is perpendicular to the detector plane, is relatively short, 37.2 Å. Images (*e–f*), exposed at an angle on the rotation spindle roughly 90° away from (*a–d*), have a quite different appearance, despite the rotation range per image being the same. Each lune is less densely populated by reflections, but the number of lunes is larger and the gaps between them much smaller. This arises from the lunes now being parallel to the (*hhl*) family of planes, as the $[1\bar{1}0]$ vector is now parallel to the beam. The interplanar spacing within this family is less than for those on

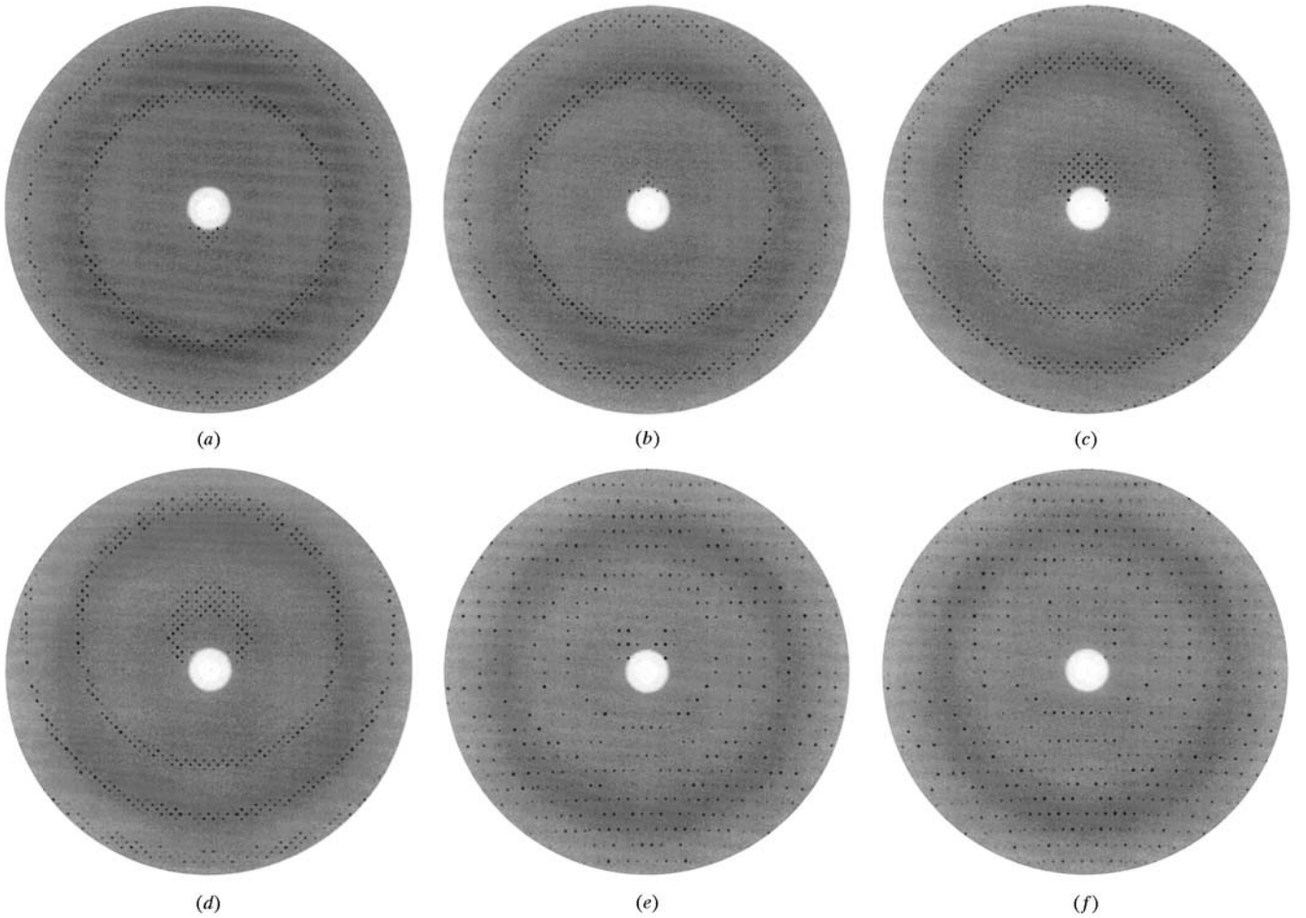

Fig. 9.1.10.1. Images recorded from a crystal of lysozyme. (*a–d*) Four consecutive exposures with the crystal fourfold axis parallel to the X-ray beam. (*e–f*) Two successive exposures 90° away, when the fourfold axis lies vertically in the plane of the image. The crystal [110] direction is parallel to the rotation axis, horizontal in the plane of the images.

references